# Usefulness of biological fingerprint in magnetic resonance imaging for patient verification

上田, 康之

https://doi.org/10.15017/1654742

出版情報：九州大学, 2015, 博士（保健学）, 課程博士
バージョン：

# Usefulness of biological fingerprint in magnetic resonance imaging for patient verification

Yasuyuki Ueda[1,2], Junji Morishita[3], Shohei Kudomi[2], Katsuhiko Ueda[3],

1. *Department of Health Sciences, Graduate School of Medical Sciences, Kyushu University, 3-1-1 Maidashi, Higashi-ku, Fukuoka, Japan*
2. *Department of Radiological Technology, Yamaguchi University Hospital, 1-1-1, Minamikogushi, Ube, Yamaguchi, Japan,*
3. *Department of Health Sciences, Faculty of Medical Sciences, Kyushu University, 3-1-1 Maidashi, Higashi-ku, Fukuoka, Japan*

Corresponding Author:

Yasuyuki Ueda,

e-mail: ueda.y.003@s.kyushu-u.ac.jp

tel: +81836222720

fax: +81836222635

The total number of words of the manuscript, including entire text from title page to figure legends: **5444**

The number of words of the abstract: **182**

The number of figures: **6**

The number of tables: **3**

# Abstract

The purpose of our study is to investigate the feasibility of automated patient verification using multi-planar reconstruction (MPR) images generated from three-dimensional magnetic resonance (MR) imaging of the brain. Several anatomy-related MPR images generated from three-dimensional fast scout scan of each MR examination were used as biological-fingerprint images in this study. The database of this study consisted of 730 temporal pairs of MR examination of the brain. We calculated the correlation value between current and prior biological-fingerprint images of the same patient and also all combinations of two images for different patients to evaluate the effectiveness of our method for patient verification. The best performance of our system were as follows: a half-total error rate of 1.59% with a false acceptance rate of 0.023% and a false rejection rate of 3.15%, an equal error rate of 1.37%, and a rank-one identification rate of 98.6%. Our method makes it possible to verify the identity of the patient using only some existing medical images without the addition of incidental equipment. Also, our method will contribute to patient misidentification error management caused by human errors.



# Key words

*Biological fingerprint, Biometrics, patient verification, MRI, scout image, patient safety,*

# 1. Introduction

Patient misidentification error management is one of the important factors of patient safety [1-8]. Positive patient verification is essential to avoid patient misidentification and for the prevention of malpractice, which includes accidents in medication, blood transfusion, surgical intervention, as well as wrong patient examinations [2-5]. The most commonly used patient verification procedure requires confirmation of the patient medical record number (MRN) or the patient-specific information (e.g. name or date of birth) on an identification band or the patient's own verbal confirmation [4,5]. Although there has been considerable research on this management issue [2-5], these processes have the possibility of patient misidentification risk caused by human mistakes [5-7] and system problems [8]. The confirmation of MRN or specific information is not possible for comatose patients [5,6]. When a patient has some identification documents and is unable to communicate, it is difficult to verify the correct information due to insufficiency of patient information. Moreover, after the finish of an examination, we have no way of confirming whether the registered patient information is correct or not. Thus, it is necessary to confirm the registered patient information by using other non-verbal approaches and to verify registered patient information even after the finish of an examination, such as biometrics. Biometric verification has a potential to be a good alternative to current verification practices [1,9,10].

Biometrics has been widely applied to identification and verification techniques in many fields over the years. Biometrics refers to technologies that measure and analyze human body characteristics [11], such as DNA, fingerprints, palms, eye retinas and irises, facial patterns, vein structure, physiological signals [12-16], and medical images [17-22]. An example of an application of medical images would be automated patient identification based on biological fingerprints in chest radiographs [17-20]. This technique has the advantage of identifying a patient through search by image as well as enabling the linking of medical exam results to the correct patient information. To expand the range verification, we applied it to magnetic resonance (MR) imaging of the brain.

Recently, a low-resolution fast three-dimensional (3D) scout scan was developed that includes several automatically-computed multi-planar reconstruction (MPR) images including anatomical reference positions and orientations based on landmark detection or a statistical model [23,24]. MPR images used as a localizer provide an operator with high intra-patient reproducibility and high inter-patient robustness in setting scan plane [23]. We predicted that MPR images with a robust and accurate reference would be useful for automated patient identification by comparing each corresponding plane. The purpose of our study is to investigate the feasibility of automated patient identification using multi-planar reconstructed MR imaging of the brain.

# 2. Methods

## 2.1 Subjects

This study was conducted as a retrospective, observational study, and was approved by the Institutional Review Board at Yamaguchi University Hospital. All the procedures followed in the study were in accordance with the Declaration of Helsinki.

We constructed a database containing to two different examination sets of scout multi-planer reconstruction image data for each patient - a prior examination and a current or recent one. This study uses the scan information of 730 patients.

Patient characteristics were as follows: 352 males and 358 females, mean age: 58 years old (range 20-80 years old). The details of each scan interval between the prior and current examinations were as follows: from 1 day to 1 week in 87 patients, from 1 week to 1 month in 103 patients, from 1 month to 3 months in 124 patients, from 3 months to 6 months in 124 patients, from 6 months to 1 year in 156 patients, and from 1 year to 3 years in 136 patients. The clinical results for the brain magnetic resonance (MR) imaging finding were as follows: brain tumor in 296 patients, cerebrovascular angiopathy in 292 patients, other brain diseases in 124 patients and nothing particular in 33 patients. Nineteen have a plurality of diseases. The types of treatment for brain disease that the patients underwent between the prior examination and the current examination are as follows: surgical operation in 72 patients, internal treatment in 51 patients and follow-up with no particular treatment in 607 patients, who have already been treated before the prior examination with the following: surgical operation in 96 patients, internal treatment in 43 patients and other treatments in 468 patients. All patient information used in this study was provided by Yamaguchi University Hospital from the time period April 2011 to March 2014. The scout acquisition protocol uses the Volumetric Interpolated Breath-hold Examination (VIBE) sequence to scan T1-weighted three-dimensional (3D) volume on a 3.0T MR system (MAGNETOM Skyra, SIEMENS, Erlangen, Germany) equipped with a 20-channel head and neck coil (Head/Neck 20, SIEMENS, Erlangen, Germany) using the following parameters: 3.15 ms of repetition time, 1.37 ms of echo time with an 8-degree flip angle. Each slice contains 162 × 162 pixels and has a typical field of view of 260 × 260 $mm^2$, yielding an

in-plane spatial resolution of 1.6 × 1.6 $mm^2$ and a slice thickness of 1.6 mm for the scout 3D volumes in the sagittal plane. From each 3D volume of whole brain, several brain anatomical positions and orientations are computed and eleven MPR images with an in-plane spatial resolution of 1.6 × 1.6 $mm^2$ and a slice thickness of 1.6 mm are reconstructed by using the AutoAlign® head algorithm [23]. Reference lines corresponding to the scout MPR images are illustrated in **Fig.1**.

## 2.2 Methodology

**Figure 2** shows the flowchart for the biological-fingerprint image creation process of our method. Let $I_0(n)$ and $T_0(n)$ be the pixel values of two MPR images corresponding to the input (current) and the template (prior) MPR images, respectively.

In the first procedure, to obtain the direction and quantity of displacement of $I_0(n)$ from $T_0(n)$, the two-dimensional cross-correlation between $I_0(n)$ and $T_0(n)$ is computed, and it is decided that the images coincide at a coordinate where a cross-correlation value is maximum. $I_0(n)$ is processed for translation so as to cancel that displacement, and $I'(n)$ is obtained. Note that all of MPR images have equivalent scale so that it is unnecessary to apply to the scale correction between $I_0(n)$ and $T_0(n)$. Second, in order to analogize left and right side head neck areas by evaluating their partial resemblance, the MPR images (d), (e), (f), (g), (h) and (i) are divided into left part and right part images along the midsagittal plane (c), and also the left and right MPR images (a) and (b) are respectively assigned as a left part and right part images. This process does nothing when the MPR image is the midsagittal, (c). Third, the image banalization technique was executed for all pixels that had greater than minimum value in both $I'(n)$ and $T_0(n)$ and a masking region was obtained. Subsequently, a left part with masking image, $I_{m,lt}(n)$, and a right part with masking image, $I_{m,rt}(n)$, were respectively applied with the thresholding technique using the masking region to $I_{rt}(n)$ and $I_{lt}(n)$. Similarly, a left part with masking image, $T_{m,lt}(n)$, and a right part with masking image, $T_{m,rt}(n)$, were also obtained. The processing above is applied to all MPR images, and eight pair images $(a_{m,rt},a_{m,lt})$, $(b_{m,rt},b_{m,lt})$, $(d_{m,rt},d_{m,lt})$, $(e_{m,rt},e_{m,lt})$, $(f_{m,rt},f_{m,lt})$, $(g_{m,rt},g_{m,lt})$, $(h_{m,rt},h_{m,lt})$ and $(i_{m,rt},i_{m,lt})$ and a single image $(c_m)$ is obtained as a biological-fingerprint image.

Let $I(n)$ and $T(n)$ be the pixel values of two biological-fingerprint images corresponding to the input and the template images, respectively. To examine the resemblance for each corresponding biological-fingerprint image between $I(n)$ and $T(n)$, we determined the correlation value, $r$, by the following formula:

$$r = \frac{1}{N}\sum_{n=1}^{N}\frac{\left\{I(n)-\bar{I}\right\}\left\{T(n)-\bar{T}\right\}}{\sigma_I \cdot \sigma_T}, \quad (1)$$

where

$$\bar{I} = \frac{1}{N}\sum_{n=1}^{N} I(n),$$

$$\bar{T} = \frac{1}{N}\sum_{n=1}^{N} T(n), \quad (2)$$

$$\sigma_I = \sqrt{\frac{\sum_{n=1}^{N}\left\{I(n)-\bar{I}\right\}^2}{N}},$$

$$\sigma_T = \sqrt{\frac{\sum_{n=1}^{N}\left\{T(n)-\bar{T}\right\}^2}{N}}.$$

$N$ is the number of masking region pixels which have a value greater than minimum value among all pixels in both $I(n)$ and $T(n)$. That is, when masking region pixel values are not available, they will be excluded from the correlation computation. The correlation value is a number from 0.0 to 1.0. If there is no resemblance between the input and the template images, the correlation value is 0.0 or very low. As the strength of the resemblance between $I(n)$ and $T(n)$ increases, the correlation value increases toward 1.0. An absolute resemblance gives the correlation value of 1.0. In the calculation of the biological-fingerprint images ($a_{m,rt}$,$a_{m,lt}$), ($b_{m,rt}$,$b_{m,lt}$), ($d_{m,rt}$,$d_{m,lt}$), ($e_{m,rt}$,$e_{m,lt}$), ($f_{m,rt}$,$f_{m,lt}$), ($g_{m,rt}$,$g_{m,lt}$), ($h_{m,rt}$,$h_{m,lt}$), and ($i_{m,rt}$,$i_{m,lt}$), the correlation values of left part and right part are compared with each other, the higher correlation value is adopted as the similarity value of the biological-fingerprint images (*a*), (*b*), (*d*), (*e*), (*f*), (*g*), (*h*) and (*i*), respectively. In the calculation of the biological-fingerprint images ($c_m$), the correlation value is adopted as the similarity value of the biological-fingerprint image (c). The correlation values between $I(n)$ and $T(n)$ were determined for the same 730 patient pairs and also all of possible combinations of a different patient pair from the prior examination set of 730 patients.

## 2.3 Performance evaluation

The threshold value in each distribution of the same patient pair and different patient pairs were evaluated by use of the squared Mahalanobis distance [25]. The squared Mahalanobis distance, $d^2$, is defined as the following formula:

$$d^2 = \frac{(n-\mu)^2}{\sigma^2}, \quad (3)$$

where μ is the mean correlation value and $\sigma$ is the standard deviation of the distribution $n$. The threshold value is the point that is equidistant to the squared Mahalanobis distance from each correlation value distribution of same patient pair and that of different patient pair. The discriminant function, $f(n)$, utilizing the squared Mahalanobis distance to determine whether a biological-fingerprint image pair is the same patient or a different patient, is calculated by the following formula:

$$f(n) = d_s^2 - d_d^2 = \frac{(n-\mu_s)^2}{\sigma_s^2} - \frac{(n-\mu_d)^2}{\sigma_d^2}, \quad (4)$$

where $d_s$, $\mu_s$ and $\sigma_s$ belong to the same patient distribution, $d_d$, $\mu_d$ and $\sigma_d$ belong to a different patient distribution. A correlation value, C, is obtained by the method in the beginning of section 2.2.2 and is substituted into the discriminant function, $f(n)$, thus obtaining a discrimination value, $f$(C). If $f$(C) is greater than zero, the pair is from the same patient. All other values signify a different patient pair. That is, C is the threshold correlation value satisfying $f$(C) is equals to zero.

We calculated the false rejection rate (FRR), the false acceptance rate (FAR) and the half-total error rate (HTER) by the discriminant function, $f(n)$.

$$FRR = \frac{FR}{TA + FR} \quad (5)$$

$$FAR = \frac{FA}{TR + FA} \quad (6)$$

$$HTER = \frac{FRR + FAR}{TAR + FRR + TRR + FAR} \quad (7)$$

Where TA is the number of true acceptance, FR is the number of false rejection, TR is the number of true rejection, FA is the number of false acceptance, TAR is the true acceptance rate and TRR is the true rejection rate.

The overall verification performance of our method was evaluated in terms of receiver operating characteristic (ROC) curve at various threshold correlation value settings, area under the ROC curve (AUC) and its equal error rate (EER). The ROC curve shows a trade-off relationship between the TAR which represents the rate of correct verification and the FAR which represents the rate of incorrect verification as its discrimination threshold is varied. The ROC curve is also possible to compare the AUC which is integral of ROC curve. The EER is the error rate at which the FAR equals the FRR, and is a commonly accepted summary of verification performance.

The performance of our method was evaluated in terms of cumulative match characteristic (CMC) curves and its rank-one identification rates. The CMC curve is to evaluate the probability of a correct identification within the top ranked match results for closed-set identification. The rank-R identification rate is the proportion of correct match that ranked within the top R matches. That is, the rank-one identification rate represents that a correlation value of the same patient pair is higher than that of all different patient pairs. The FRR is also a performance value in identifying patients.

# 3. Results

**Figure 3** shows the histograms for the correlation values of the same 730 temporal pairs and that of all combinations of two images for different patients of each biological-fingerprint image. **Figure 4** shows the error rates on the vertical axis against the threshold correlation value on the horizontal axis obtained with each biological-fingerprint analysis. Also shown in the Figure is the equal error rate (EER) achieved at the point where the false acceptance rate (FAR) and false rejection rate (FRR) are equal to each other. **Figure 5** shows the receiver operation characteristic (ROC) curves in the biological fingerprint analysis. The EERs shown in **Table 1** are also presented by the crossing between the ROC curves and equal error rate line. **Figure 6** shows the cumulative match characteristic (CMC) curves in the biological-fingerprint analysis. The rank-one identification rates shown in **Table 1** are also represented when the identification rate has the first rank in all patient comparisons.

**Table 1** shows the result of threshold correlation values and the performance values for each biological-fingerprint analysis. The threshold correlation value row shows the result of threshold correlation value obtained by using the discriminant analysis utilizing the Mahalanobis distance. For each threshold correlation value, we calculated FRR, FAR, and half-total error rate (HTER). For analysis of the ROC curve shown in **Fig. 5**, the results of EER and the area under the ROC curve (AUC) for each biological-fingerprint image are shown in the EER and AUC rows, respectively in **Table 1**. For analysis of the CMC curve for each biological-fingerprint image is shown in **Fig. 6** as the rank-one identification rate in **Table 1**.

**Table 2** shows the FRR for the types of brain treatment that the patient underwent between the prior and current examinations for each biological fingerprint analysis. All patients in this study are divided into the following three classes: surgical operation, internal treatment, and follow-up with no particular treatment. Respective follow-up with no particular treatment patients are further classed based on their brain treatment before the prior examination with the following: surgical operation, internal treatment, and other treatments or no particular treatment.

**Table 3** shows the FRR for the clinical results of the brain MR imaging finding of each biological fingerprint analysis. All patients in this study are divided into the following four classes: brain tumor, cerebrovascular angiopathy, other brain diseases, and nothing particular.

The lower the FAR, FRR, HTER, and EER, the better the biometric system is for verification. Correspondingly, a higher threshold correlation value will reduce the FAR, but increase the FRR. The higher the AUC, the better the biometric system is for verification. The higher the rank-one identification rate, the better the biometric system is for closed-set identification. Our results indicated a high performance in identifying and verifying patients. The biological-fingerprint analysis by transversal IAC has excellent verification performance, simultaneously excellent closed-set identification performance. The performance values of FRR, FAR, HTER, EER, AUC and the rank-one identification rate for biological-fingerprint analysis by transversal IAC were 3.15% , 0.023%, 1.59%, 1.37%, 0.998 and 98.6%, respectively.

It is important to note that most parts of these two curves in **Figs. 3, and 4** are separated, biological-fingerprint analysis by transversal basal ganglia image shown in **Fig. 3h** is more overlapped compared with other parts in all of the biological-fingerprint analysis. For this reason, biological-fingerprint analysis by transversal basal ganglia image indicated lower performance than that of other biological-fingerprint analysis.

As shown in **Table 2**, the FRR in 72 patients, who underwent surgical operation between the prior and current examinations, indicated lower performance than the FRR in all 730 patients. The FRR in 296 patients who have had a brain tumor indicated a slightly lower performance than the FRR in all 730 patients shown in **Table 3**.

# 4. Discussion

Our results indicated a high performance in identifying and verifying patients using various MPR images as biological-fingerprints, except for a transversal basal ganglia one. This technique based on using several anatomy-related MPR images generated from 3D scout scan of brain MR imaging as biological-fingerprint images is potentially useful for verifying the patient without any other information.

The biological-fingerprint analysis by transversal basal ganglia image has a higher correlation value for different patient pair comparisons and a lower correlation value for some same patient comparison than those of the other biological-fingerprint analyze shown in **Fig. 3**. The low performance with a transversal basal ganglia image seems to be related to the general observation that the section of transversal basal ganglia does not usually include unique image features in individual patients. However, the biological-fingerprint analysis by the transversal IAC image has the best performance for verification. Using the threshold correlation value of 0.83 makes it difficult for different patient pair to be falsely accepted. Although the higher threshold correlation value will increase the risk of refusing acceptance, the acceptance threshold, which is required for the patient verification system, is set very high and in order to achieve a low FAR. The HTER of 1.59% is found at threshold correlation value of 0.83 with 3.15% of FRR and 0.023% of FAR by using the transversal IAC image. Among the 266,085 pairs, which is the number of combinations of 730 patients taken 2, only 62 pairs discriminate to be incorrect results. That is, the other 266,023 pairs discriminate to be correct results. Our method satisfies the requirements for the biological-fingerprint patient verification system using existing medical images.

In the closed-set identification performance, a rank-one identification rate and FRR represents successful performance value. The higher the rank-one identification rate, the better the biometric system is for closed-set identification. Our method achieved a rank-one identification rate of 98.6% and a FRR of 3.15%. That is, among the 730 patients, 720 patients achieved the highest correlation value, and 707 patients (96.8%) achieved correct acceptance in all patient comparisons. When a same patient pair was

determined to be incorrect, some patient information with higher-rank results was able to be used by the analyst to select correction candidates.

As shown in **Table 2**, the FRR in 72 patients who underwent surgical operation between the prior and current examinations indicated lower performance. However, the FRR in 96 patients, who have undergone surgical operation before the prior examination, have high performance levels like the other patients. Furthermore, the FRR in 296 patients who have brain tumor indicated a slightly lower performance than the FRR in all 730 patients shown in Table 3. This is thought to result from formal change in the brain before and after surgical operation. Surgical operation for brain tumor is necessary for the following purposes: biopsy for the diagnosis of tumor type, and whole or partial removal of the tumor. In particular, surgical operation is usually the first step in treating most benign and many malignant tumors. This result indicated that the identification performance of our method is inferior only when using a patient who underwent surgical operation between prior and current examination. Furthermore, if a current examination uses different pulse sequences or different MR systems, there is a difference in image quality between prior scan and current scan. Changes to the structure of the brain due to illness or aging, and using images with different devices and resolution on the prior and current scans might affect the performance of our method.

Our study has limitations. One of the limitations of our study is that our database has a short-term follow-up period of 3 years. Another limitation is that it was a retrospective analysis performed at a single MR system. These limitations made it impossible to test our method's application possibilities in a wide range of fields. Repeated follow up research is needed over longer time periods and under a variety of conditions.

We consider this study to be innovative because it is possible to verify the identity of the patient only using some existing medical images without the addition of incidental equipment such as a biometric identification device, and keep the patient convenience intact. Our method will be invaluable for confirming whether a patient's information matches the person under MR examination or not. In particular, our method is useful when we have no other way of confirming whether the registered patient information is correct or not in the following situations requiring identity confirmation: the examinee is in a comatose state, the examinee is not present after the examination, and the

examinee does not have any identification documents. It is also important to take privacy into consideration in the administration of our method due to the fact that medical images which include personal information capable of specifying individuals.

# 5. Conclusion

We have to deal with various approaches to reduce the possibility of patient misidentification. It is becoming more and more important to obtain 3D biological fingerprint information for patient verification. Our method has the potential for discovering misfiled patient information after examination. Also, it will be useful for verifying registered patient information even if the patient is unable to communicate. We expect our method to be a key solution to patient misidentification problems.

# 6. Acknowledgments

The authors wish to thank Mr. Steven Gardner for his helpful advice and for improving our manuscript.

# 7. References


1. Pagliaro P, Turdo R, Capuzzo E (2009) Patients' positive identification systems. Blood Transfusion. 7:313-318
2. Dunn EJ, Moga PJ (2010) Patient misidentification in laboratory medicine A qualitative analysis of 227 root cause analysis reports in the veterans health administration. Archives of Pathology and Laboratory Medicine. 134:244-255
3. Danaher LA, Howells J, Holmes P, Scally P (2011) Is It Possible to Eliminate Patient Identification Errors in Medical Imaging? Journal of the American College of Radiology. 8:568-574
4. Schulmeister L (2008) Patient misidentification in oncology care. Clin J Oncol Nurs. 12:495-498
5. Bittle MJ, Charache P, Wassilchalk DM (2007) Registration-associated patient misidentification in an academic medical center: Causes and corrections. Joint Commission Journal on Quality and Patient Safety. 33:25-33
6. Henneman P (2010) Patient Identification Errors Are Common in a Simulated Setting. Ann Emerg Med. 55:503-509
7. Linda T. Kohn, Janet M. Corrigan, Molla S. Donaldson (2000) To Err is Human: Building a Safer Health System. National Academy Press. Washington, D.C.
8. Snyder ML, Carter A, Jenkins K, Fantz CR (2010) Patient misidentifications caused by errors in standard bar code technology. Clin Chem. 56:1554-1560
9. Committee WB, Council NR (2010) Biometric Recognition: Challenges and Opportunities. National Academies Press. Washington, D.C.
10. Bennardello F, Fidone C, Cabibbo S, et al (2009) Use of an identification system based on biometric data for patients requiring transfusions guarantees transfusion safety and traceability. Blood Transfusion. 7:193-203
11. Dunstone T, Yager N (2009) An introduction to biometric data analysis. In: Biometric System and Data Analysis. Springer US, Boston, MA, pp 3-26
12. Odinaka I, Lai P, Kaplan AD, O'Sullivan JA, Sirevaag EJ, Rohrbaugh JW (2012) ECG Biometric Recognition: A Comparative Analysis. IEEE Transactions on Information Forensics and Security. 7:1812-1824
13. Verma N, Rana M (2013) Biometric identification of person using ECG signal. Journal of Chemical, Biological and Physical Sciences 4:509-515

14. Tsuru K, Pfurtscheller G (2012) Brainwave biometrics: A new feature extraction approach with the cepstral analysis method. Transactions of Japanese Society for Medical and Biological Engineering. 50:162-167.
15. Kumari P, Vaish A (2015) Brainwave based user identification system: A pilot study in robotics environment. ROBOTICS AND AUTONOMOUS SYSTEMS. 65:15-23
16. Asadpour V, Towhidkhah F, Homayounpour MM (2006) Performance enhancement for audio-visual speaker identification using dynamic facial muscle model. Med Biol Eng Comput. 44:919-30
17. Morishita J, Katsuragawa S, Kondo K, Doi K (2001) An automated patient recognition method based on an image-matching technique using previous chest radiographs in the picture archiving and communication system environment. Med Phys. 28:1093-1097
18. Morishita J, Katsuragawa S, Sasaki Y, Doi K (2004) Potential usefulness of biological fingerprints in chest radiographs for automated patient recognition and identification. Acad Radiol. 11:309-315
19. Morishita J, Watanabe H, Katsuragawa S, et al (2005) Investigation of misfiled cases in the PACS environment and a solution to prevent filing errors for chest radiographs. Acad Radiol. 12:97-103
20. Toge R, Morishita J, Sasaki Y, Doi K (2013) Computerized image-searching method for finding correct patients for misfiled chest radiographs in a PACS server by use of biological fingerprints. Radiological Physics and Technology. 6:437-443
21. Shamir L (2013) MRI-based knee image for personal identification. International Journal of Biometrics. 5:113-125
22. Shamir L, Ling S, Rahimi S, Ferrucci L, Goldberg IG (2009) Biometric identification using knee X-rays. International Journal of Biometrics. 1:365-370
23. Chen T, Zhan Y, Zhang S, Dewan M (2011) Automatic alignment of brain MR scout scans using data-adaptive multi-structural model. In: Gabor F, Anne M, Terry P (eds) Medical Image Computing and Computer-Assisted Intervention - MICCAI 2011. Springer Berlin Heidelberg, Berlin, pp 574-581
24. van der Kouwe AJW, Benner T, Fischl B, et al (2005) On-line automatic slice positioning for brain MR imaging. Neuroimage. 27:222-230
25. Mahalanobis PC (1936) On the generalized distance in statistics. Proceedings National Institute of Science of India. 2:49-55

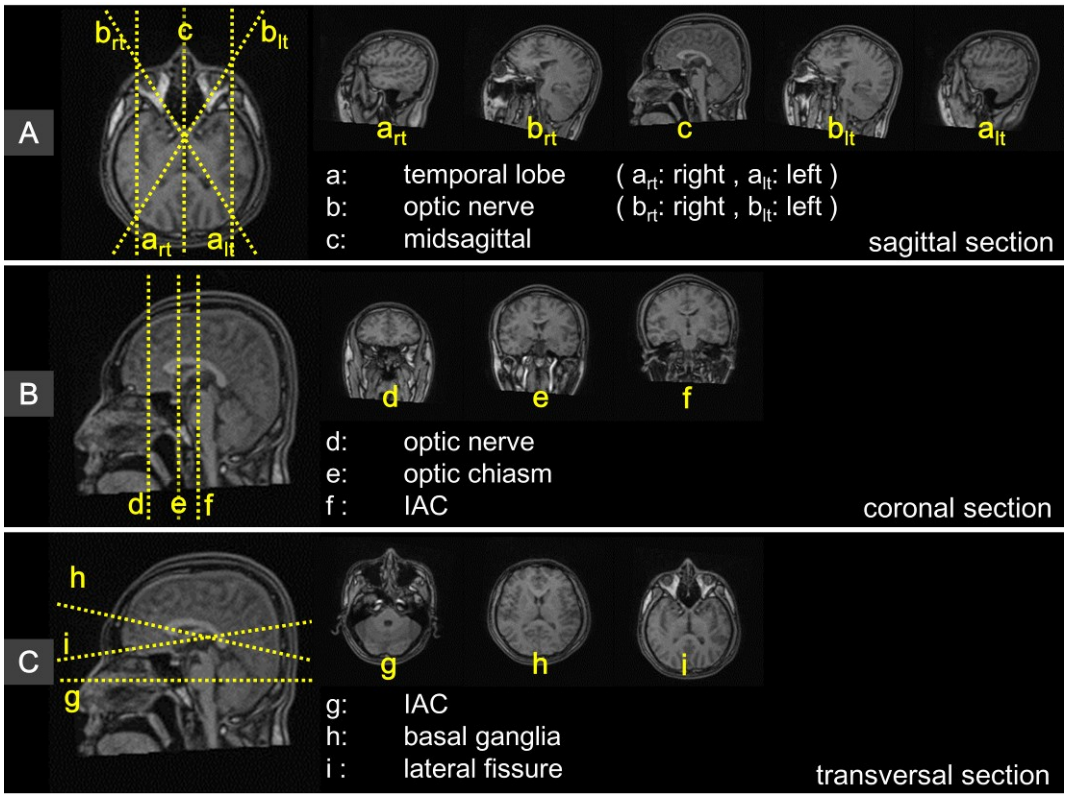


**Figure 1**

**Reference lines and corresponding to the scout MPR images**

A is a transversal image through the lateral fissure showing reference lines (yellow lines) and five corresponding oblique sagittal MPR images: (*a*) temporal lobe ($a_{rt}$: right and $a_{lt}$: left), (*b*) optic nerve ($b_{rt}$: right and $b_{lt}$: left), and (*c*) midsagittal. B is a sagittal image through the midline showing reference lines (yellow lines) and three corresponding oblique coronal MPR images: (*d*) optic nerve, (*e*) optic chiasm, and (*f*) internal auditory canal (IAC). C is a sagittal image through the midline showing reference lines (yellow lines) and three corresponding oblique axial MPR images: (*g*) IAC, (*h*) basal ganglia, and (*i*) lateral fissure.

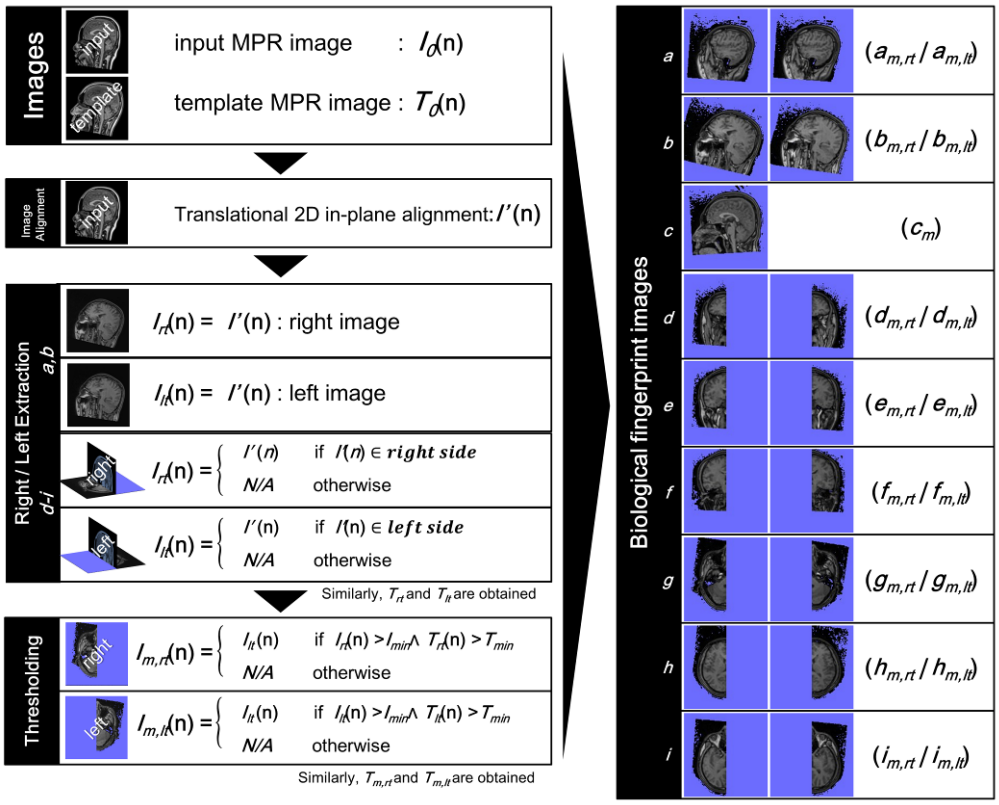


**Figure 2**

**Flowchart for the biological fingerprint image creation process**

$I_0$ and $T_0$ are the input and template MPR images, respectively. $I'$ is processed from the image registration for $I_0$. $I_{rt}$ and $I_{lt}$ are the right- and left-side MPR images of $I'$, respectively. $T_{rt}$ and $T_{lt}$ are the right- and left-side MPR images of $T_0$, respectively. $I_{m,rt}$ are greater than $I_m$ among all $I_{rt}$ pixels and greater than $T_m$ among all $T_{rt}$ pixels. Where $I_m$ and $T_m$ are the minimum value among all pixels of $I'$ and $T_0$, respectively. $I_{m,lt}$, $T_{m,rt}$, and $T_{m,lt}$ are obtained similarly.

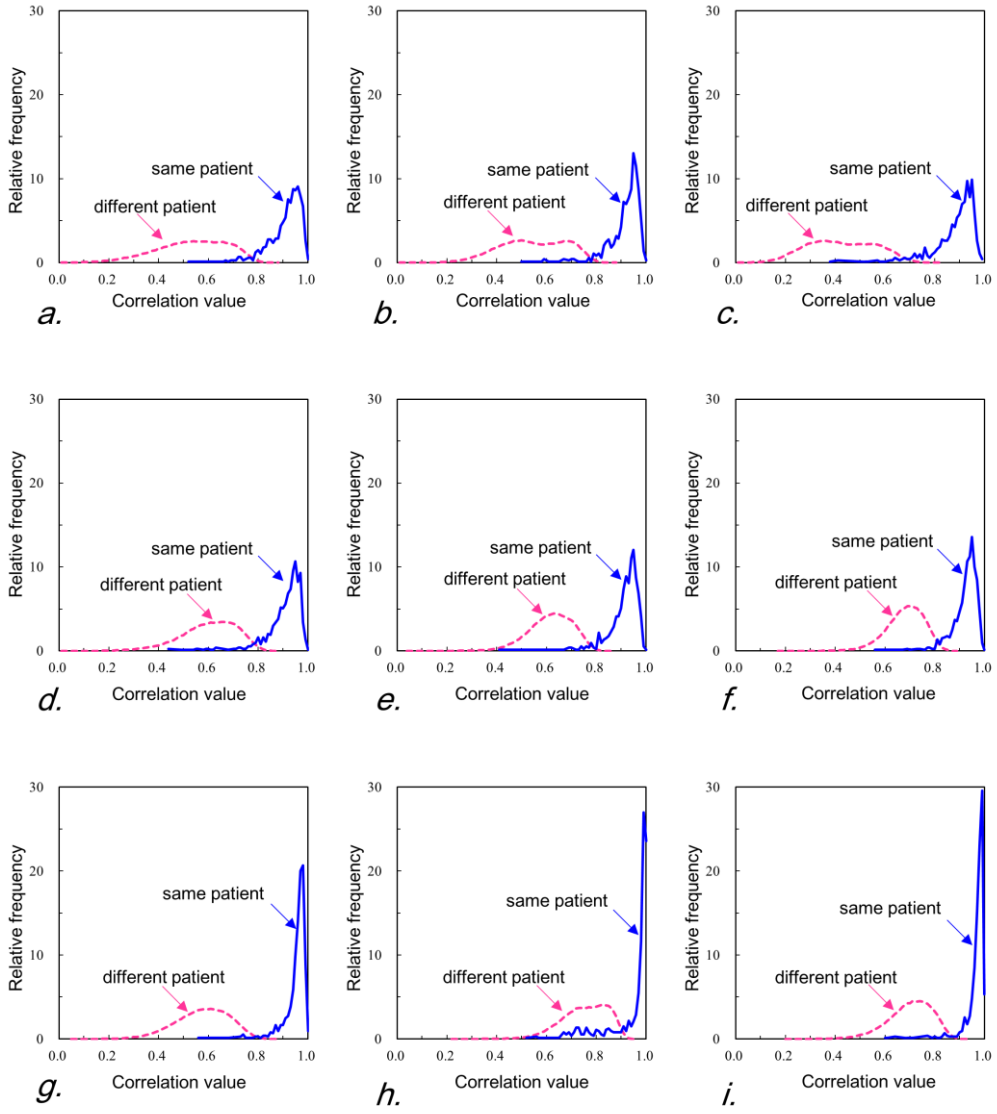


**Figure 3**

**Correlation value histogram comparison of each biological fingerprint analysis**

Histograms for correlation values between current and prior biological fingerprint images for the same patient comparisons (solid lines) and different patients comparisons (dashed lines) in terms of (*a*) sagittal temporal lobe, (*b*) sagittal optic nerve, (*c*) midsagittal, (*d*) coronal optic nerve, (*e*) coronal optic chiasm, (*f*) coronal internal auditory canal (IAC), (*g*) transversal IAC, (*h*) transversal basal ganglia, and (*i*) transversal lateral fissure.

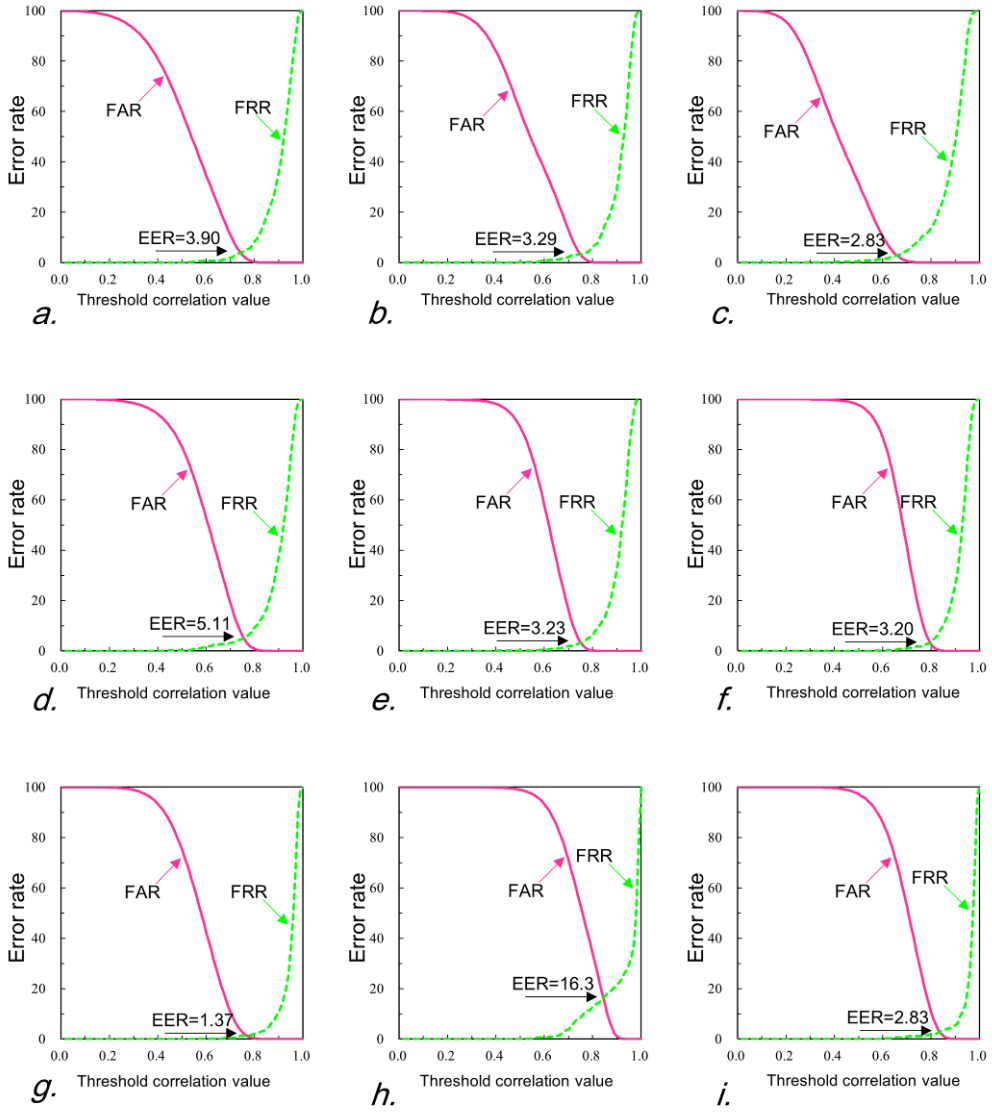


**Figure 4**

**Variation of FAR and FRR in relation to the threshold correlation value and EER of each biological fingerprint analysis**

The false acceptance rate (FAR: solid lines) and the false rejection rate (FRR: dashed line) on the vertical axis against the threshold correlation value on the horizontal axis and an arrow indicating a point of equal error rate (EER) in terms of (*a*) sagittal temporal lobe, (*b*) sagittal optic nerve, (*c*) midsagittal, (*d*) coronal optic nerve, (*e*) coronal optic chiasm, (*f*) coronal internal auditory canal (IAC), (*g*) transversal IAC, (*h*) transversal basal ganglia, and (*i*) transversal lateral fissure.

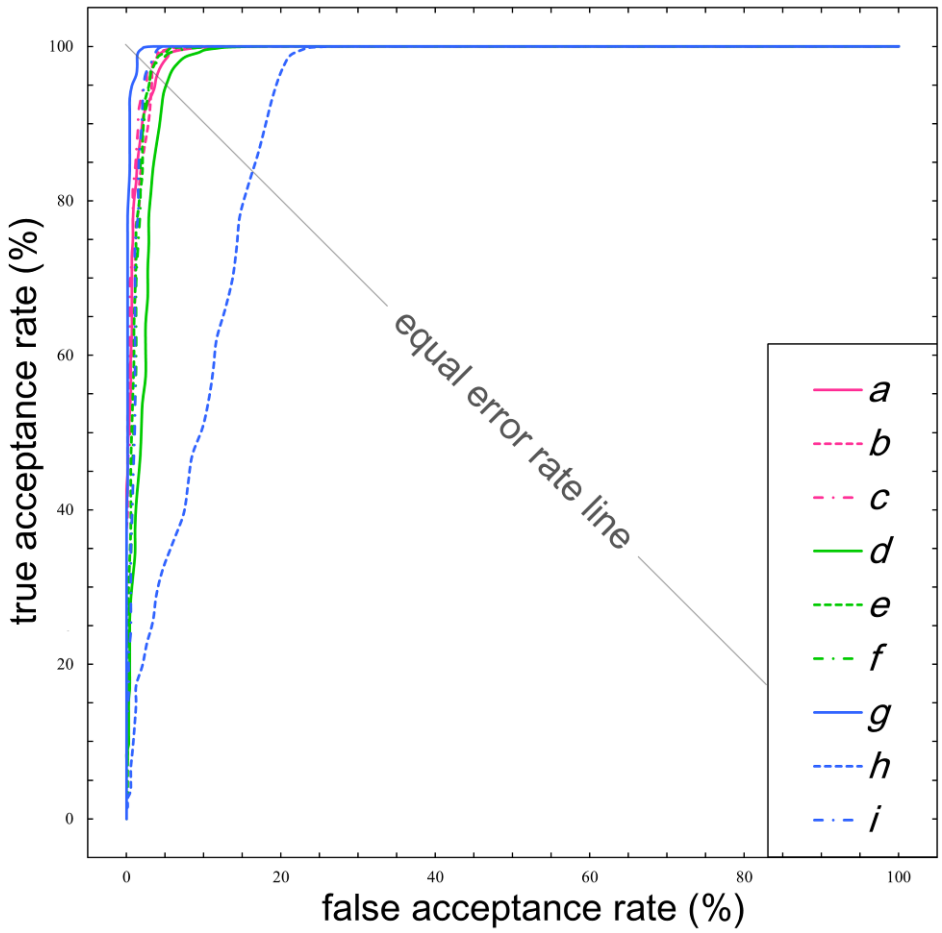


**Figure 5**

**Comparison of ROC curve performance in the biological fingerprint analysis**

Receiver operating characteristic (ROC) curves of the automated patient verification method in terms of (*a*) sagittal temporal lobe, (*b*) sagittal optic nerve, (*c*) midsagittal, (*d*) coronal optic nerve, (*e*) coronal optic chiasm, (*f*) coronal internal auditory canal (IAC), (*g*) transversal IAC, (*h*) transversal basal ganglia, and (*i*) transversal lateral fissure. The equal error rates are the points where the equal error rate line intersects an ROC curve.

The transversal IAC analysis had the most excellent ROC curve performance. The transversal basal ganglia analysis had the most inferior ROC curve performance.

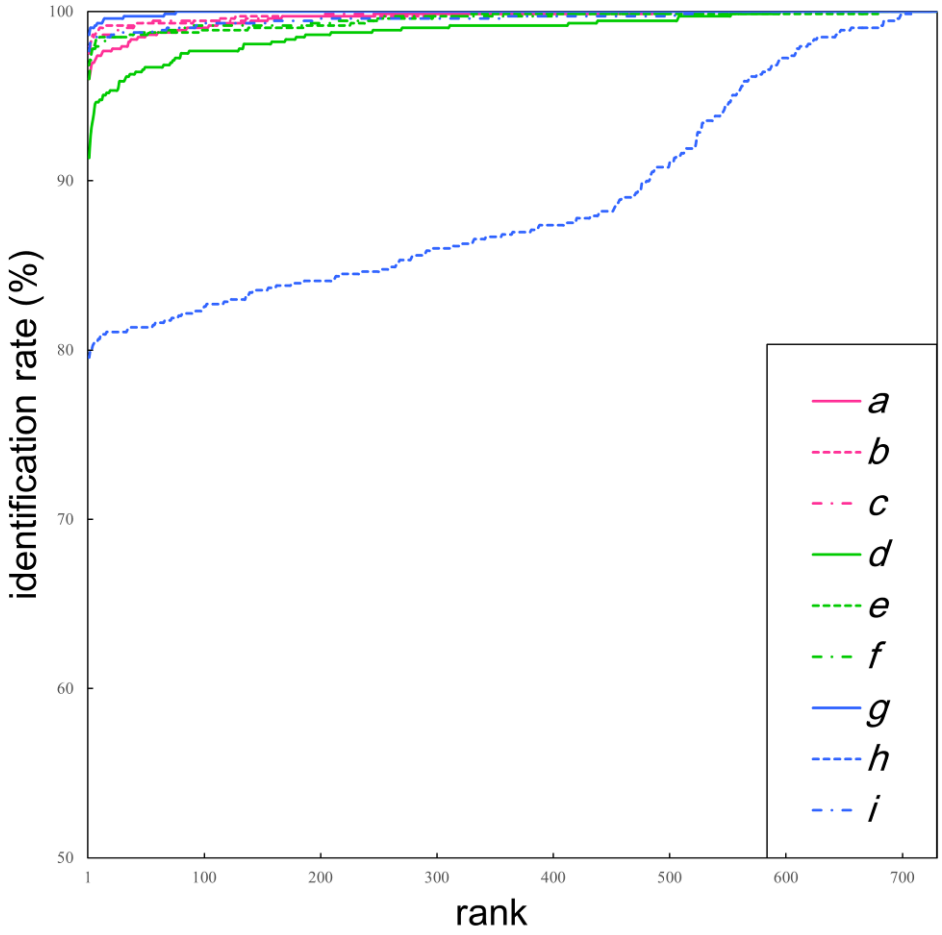


**Figure 6**

**Comparison of CMC curve performance in the biological fingerprint analysis**

Cumulative match characteristic (CMC) curves of the automated patient identification method in terms of (*a*) sagittal temporal lobe, (*b*) sagittal optic nerve, (*c*) midsagittal, (*d*) coronal optic nerve, (*e*) coronal optic chiasm, (*f*) coronal internal auditory canal (IAC), (*g*) transversal IAC, (*h*) transversal basal ganglia, and (*i*) transversal lateral fissure.

The transversal IAC analysis had the most excellent CMC curve performance. The transversal basal ganglia analysis had the most inferior CMC curve performance.

**Table 1**

**Threshold correlation value, FRR, FAR, HTER, EER, AUC and rank-one identification rate comparison of each biological fingerprint analysis**

| | Biological fingerprint | Threshold correlation value | FRR[1](%) | FAR[2](%) | HTER[3](%) | EER[4](%) | AUC[5] | rank-one identification rate (%) |
|---|---|---|---|---|---|---|---|---|
| *sagittal* | *temporal lobe* | 0.78 | 5.62 | 0.89 | 3.25 | 3.90 | 0.992 | 96.0 |
| | *optic nerve* | 0.79 | 4.66 | 0.58 | 2.62 | 3.29 | 0.991 | 97.9 |
| | *midsagittal* | 0.70 | 4.66 | 0.69 | 2.67 | 2.83 | 0.994 | 97.5 |
| *coronal* | *optic nerve* | 0.77 | 6.30 | 2.68 | 4.49 | 5.11 | 0.979 | 91.4 |
| | *optic chiasm* | 0.78 | 5.07 | 0.66 | 2.86 | 3.23 | 0.990 | 96.8 |
| | *IAC* | 0.82 | 5.21 | 1.08 | 3.14 | 3.20 | 0.988 | 96.0 |
| *transversal* | *IAC* | 0.83 | 3.15 | 0.023 | 1.59 | 1.37 | 0.998 | 98.6 |
| | *basal ganglia* | 0.84 | 16.0 | 17.7 | 16.9 | 16.3 | 0.907 | 79.6 |
| | *lateral fissure* | 0.87 | 4.11 | 0.28 | 2.19 | 2.83 | 0.990 | 97.7 |

[1]FRR: false rejection rate; [2]FAR: false acceptance rate; [3]HTER: half-total error rate; [4]EER: equal error rate; [5]AUC: area under the receiver operating characteristic curve;

The biological-fingerprint analysis by transversal internal auditory canal (IAC) had the best verification and identification performance. The biological-fingerprint analysis by transversal basal ganglia had the poorest inferior verification and identification performance.

Table 2

**False rejection rates for the types of brain treatment that the patient underwent between the prior and current examination of each biological fingerprint analysis**

| | Biological fingerprint | surgical operation (72) | internal treatment (51) | follow-up with no particular treatment (607) | | | all patients (730) |
|---|---|---|---|---|---|---|---|
| | | | | surgical operation (96) | internal treatment (43) | no particular or other treatments (468) | |
| *sagittal* | *temporal lobe* | 22.2 | 9.80 | 4.17 | 2.33 | 3.21 | 5.62 |
| | *optic nerve* | 29.2 | 5.88 | 4.17 | 0 | 1.28 | 4.66 |
| | *midsagittal* | 22.2 | 7.84 | 0 | 0 | 2.99 | 4.66 |
| *coronal* | *optic nerve* | 20.8 | 9.80 | 5.21 | 0 | 4.49 | 6.30 |
| | *optic chiasm* | 27.8 | 3.92 | 4.17 | 2.33 | 2.14 | 5.07 |
| | *IAC* | 25.0 | 7.84 | 2.08 | 2.33 | 2.78 | 5.21 |
| *transversal* | *IAC* | 16.7 | 1.96 | 3.13 | 0 | 1.50 | 3.15 |
| | *basal ganglia* | 16.7 | 13.7 | 19.8 | 14.0 | 15.6 | 16.0 |
| | *lateral fissure* | 30.6 | 3.92 | 2.08 | 0 | 0.85 | 4.11 |

Numbers in parentheses indicate the numbers of each object patients.

The FRR in 72 patients, who underwent surgical operation between the prior and current examinations, indicated lower performance than the FRR in all 730 patients. However, the FRR in 96 patients, who underwent surgical operation before the prior examination, had high performance levels like the other patients.

Table 3

**False rejection rates for the clinical results of the brain magnetic resonance imaging finding of each biological fingerprint analysis**

| | Biological fingerprint | tumor (296) | angiopathy (292) | other diseases (124) | no particular (33) | all patients (730) |
|---|---|---|---|---|---|---|
| *sagittal* | *temporal lobe* | 6.76 | 4.45 | 8.87 | 3.03 | 5.62 |
| | *optic nerve* | 9.12 | 1.37 | 3.23 | 3.03 | 4.66 |
| | *midsagittal* | 7.09 | 2.74 | 5.65 | 3.03 | 4.66 |
| *coronal* | *optic nerve* | 7.09 | 4.45 | 9.68 | 9.09 | 6.30 |
| | *optic chiasm* | 7.77 | 4.11 | 3.23 | 3.03 | 5.07 |
| | *IAC* | 7.43 | 4.11 | 4.84 | 3.03 | 5.21 |
| *transversal* | *IAC* | 4.39 | 2.05 | 3.23 | 3.03 | 3.15 |
| | *basal ganglia* | 15.2 | 19.2 | 16.1 | 9.09 | 16.0 |
| | *lateral fissure* | 7.77 | 1.71 | 2.42 | 3.03 | 4.11 |

Numbers in parentheses indicate the numbers of each object patients.

The FRR in 296 patients who have had a brain tumor indicated a slightly lower performance than the FRR in all 730 patients.

## All the Author's Biography

**YASUYUKI UEDA** was born in Fukuoka, Japan, in 1979. He received the associate degree in health science from the Kyushu University School of Health Science, Japan, in 2005, and he has been working at Yamaguchi University Hospital as a Radiological Technologist since 2005. Since 2013, he has also been a Ph.D. course student at the Kyushu University Graduate School of Medical Sciences.

His current research interests include magnetic resonance imaging, computed tomography, molecular imaging, digital image processing, medical information systems, and biometrics.

---

**JUNJI MORISHITA** received Ph.D. degree from Gifu University in 1997. He is currently a Professor in the Department of Health Sciences, Kyushu University. His research interests include image matching, and image evaluation in medicine.

---

**SHOHEI KUDOMI** was born in Fukuoka, Japan, in 1981. He received the M.Sc. degree in health science from the Kanazawa University Graduate School of Medical Sciences, Japan, in 2011, and he has been working at Yamaguchi University Hospital as a Radiological Technologist since 2004. Since 2011, he has also been a Ph.D. course student at Kanazawa University Graduate School of Medical Sciences.

His current research interests include computed tomography, radiation dose reduction, and image evaluation.

---

**KATSUHIKO UEDA** received the associate degree in health science from the Kyushu University School of Health Science, Japan, in 1982, and he has been working at Yamaguchi University Hospital as Chief of Radiological Technologist since 2009.

His current research interests include evaluation of medical X-ray image property and X-ray energy control for medical image.